Photon-Modulated Bond Covalency of [Sm(II)(η^9-C_9H_9)$_2$]

T. Vitova,* H. Ramanantoanina, B. Schacherl, L. Münzfeld, A. Hauser, R. S. K. Ekanayake, C. Y. Reitz, T. Prüßmann, T. S. Neill, J. Göttlicher, R. Steininger, V. A. Saveleva, M. W. Haverkort, and P. W. Roesky

ABSTRACT: Lanthanides are widely assumed not to form covalent bonds due to the localized nature of their 4f valence electrons. This work demonstrates that the ionic bond of Sm(II) with cyclononatetraenyl (η^9-$C_9H_9^-$) in [Sm(η^9-C_9H_9)$_2$] can be modulated and becomes more covalent by photon-induced transfer of Sm 4f electrons to Sm 5d orbitals. This photon-induced change in bonding properties facilitates a subsequent reconfiguration of [Sm(η_9-C_9H_9)$_2$]. As a result, Sm−C bond length contraction is detected and the local Sm coordination environment exhibits more extensive disorder. Both Sm 4f and 5d electrons have increased participation in covalent Sm−ligand interactions. The Sm L_3-edge valence band resonant inelastic X-ray scattering (VB-RIXS), high-resolution X-ray absorption near-edge structure (HR-XANES), and quantum chemical computations showcase a spectroscopic methodology for in-depth studies of bond covalency of lanthanide atoms.

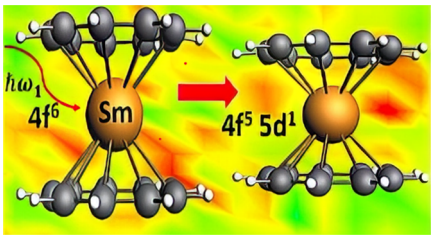

INTRODUCTION

The lanthanide elements (Ln) have established technological importance due to their magnetic, luminescence, electronic, and catalytic properties.[1−4] Despite many advances, there are still significant, fruitful areas in Ln chemistry and physics to further develop.[5,6] Ln 4f valence electrons are typically described as localized, and Ln ions are stable predominantly in their +III oxidation states and form ionic chemical bonds. In the past decade, materials in which Ln exhibits intermediate oxidation states, form covalent chemical bonds, or stabilize the +II oxidation state across the entire 4f series have become more accessible.[7−15] We recently reviewed some of the open questions related to the chemical binding of lanthanide atoms.[14]

The classical definition of a covalent bond is the accumulation of electron density between two bonding atoms. In this case, the valence orbitals of the metal mix with the valence orbitals of the ligand.[16] For Ln, those are the 4f, 6s and, for some Ln, the 5d orbitals.[7,8,10,13,15] Ce is one prominent example of forming covalent bonds with its 4f and 5d orbitals, leading to rich physical and chemical properties,[7,8,10] such as the emission of luminescence with adjustable wavelengths. Tunable emission can be accomplished when binding Ce to different ligands, resulting in variable Ce−ligand bonding properties. There are examples in the literature of Ln(III) 5d orbitals being involved in covalent bonds.[7,8] Those are more readily accessible than 4f orbitals due to the extended radial distribution of the 5d orbitals. It is also possible for most Ln elements to access the +II oxidation state by transferring an electron from the ligand to the metal 5d orbitals and thus obtaining Ln(II) with higher potential for forming covalent bonds.[9] It was previously shown that irradiation with visible light can enhance the reactivity of Sm(II) by inducing $4f^6 \rightarrow 4f^5 5d^1$ transition.[17−19] However, how these changes in the valence electron configuration and reactivity are related to changes in bonding properties of Sm(II) was not identified. Tuning the electronic properties of Ln will provide opportunities to better understand the degree of covalency of their chemical bonds. As a result, enhanced reactivity and novel chemical and electronic properties of Ln and their complexes can become available.

Herein, we focus on the covalency of the Ln−ligand bonds and demonstrate a way to modulate them. We specifically probe Sm, which has nominally 4f, 6s, and no 5d electrons ($4f^6 6s^2$ valence electron configuration for Sm in 0 oxidation state). With careful synthesis, Sm can be stabilized as Sm(II), a species of high interest in small molecule activation and catalysis.[20] Using a multitechnique spectroscopic approach, it will first be demonstrated that Sm(III) forms covalent bonds in the solid compound Sm_2O_3. We will then illustrate that the molecular Sm(II) compound [Sm(η^9-C_9H_9)$_2$][21] (cyclononatetraenyl ligand, η^9-$C_9H_9^-$)[21] can be used as an electron pump, driven by X-rays to pump valence Sm 4f electrons to 5d orbitals, which can then participate in covalent bonding. The large η^9-C_9H_9 ring stabilizes the highly reactive Sm(II) center, which facilitates the handling. Our study is the first example of a covalent Sm(II) molecular compound with a $4f^5 5d^1$ valence configuration. Finally, we will showcase the application of valence band high-energy resolution resonant inelastic X-ray

scattering (VB-RIXS) and high-resolution X-ray absorption near-edge structure (HR-XANES) as probes of Ln−ligand bond covalency.

RESULTS AND DISCUSSION

Bond Covalency in the Crystalline Solid Compound Sm_2O_3.

Sm L_3-edge HR-XANES of Sm_2O_3. We first probe the electronic structure of Sm in crystalline Sm_2O_3 by Sm L_3-edge HR-XANES (process described in Figure 1).[22−26] Figure 2

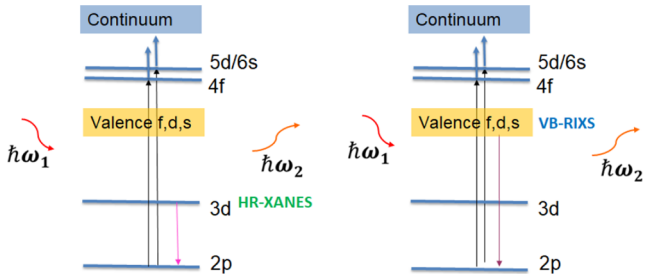

Figure 1. Schematic representations of the electronic transitions involved in the Ln L_3-edge HR-XANES (left) and VB-RIXS (right) experimental techniques following selection rules $\Delta l = \pm 1$, $\Delta J = 0$, and ± 1.

depicts the experimental Sm L_3-edge HR-XANES compared to the computed spectrum (a) and the calculated Sm d, s, and f-density of states (DOS) (b). Sm(III) is present in Sm_2O_3, resulting in $4f^5 6s^0 5d^0$ electron configuration. The HR-XANES spectrum probes the unoccupied d-DOS of Sm, following the dipole section rule $\Delta l = \pm 1$, $\Delta J = 0$, and ± 1 obeyed by the electron transitions (2p → 5d/6s, cf. Figure 1). The pre-edge feature, resolved only due to the high experimental energy resolution applied here, corresponds to the energy position of the 4f orbitals in the DOS. This transition is weak but gains intensity in HR-XANES due to hybridization of 4f and 5d Sm orbitals because of the lack of local inversion symmetry.

The calculated spectrum describes all experimental spectral features with only minor deviations in the energy positions and broadening. It has intensity in the pre-edge region only when dipole transitions are considered (peak A in Figure 2a), confirming the mixing of 5d/6s and 4f orbitals. The intensity of peak A increases when quadrupole transitions to 4f orbitals are also considered (2p → 4f). Mixing of the O 2p and Sm 5d/6s states, including a small 4f contribution, is evident for the unoccupied and occupied orbitals, suggesting a major participation of 5d/6s orbitals in Sm−O covalent bonding in Sm_2O_3.

Sm L_3-edge VB-RIXS of Sm_2O_3. We applied Sm L_3-edge VB-RIXS as an experimental probe of the 5d and 6s electron density of Sm in the occupied valence band and their participation in Sm−O bonding.[27] The principle of this experimental technique includes excitation of 2p electrons to the unoccupied 5d states and the subsequent X-ray emission caused by 5d and 6s Sm electrons from the valence band filling the 2p core-hole, which is detected with high experimental energy resolution using a spectrometer (cf. Figure 1). The intense peak of the VB-RIXS spectrum is due to an excitation process, where the excited electron fills the created core−hole (elastic peak). The first peak B at 0 to −5 eV arises from the Sm 6s and 5d electron density in the valence band (cf. Figure 2c). Given that Sm(III) formally has the electronic configuration $4f^5 6s^0 5d^0$, if Sm−O bonding was wholly ionic,

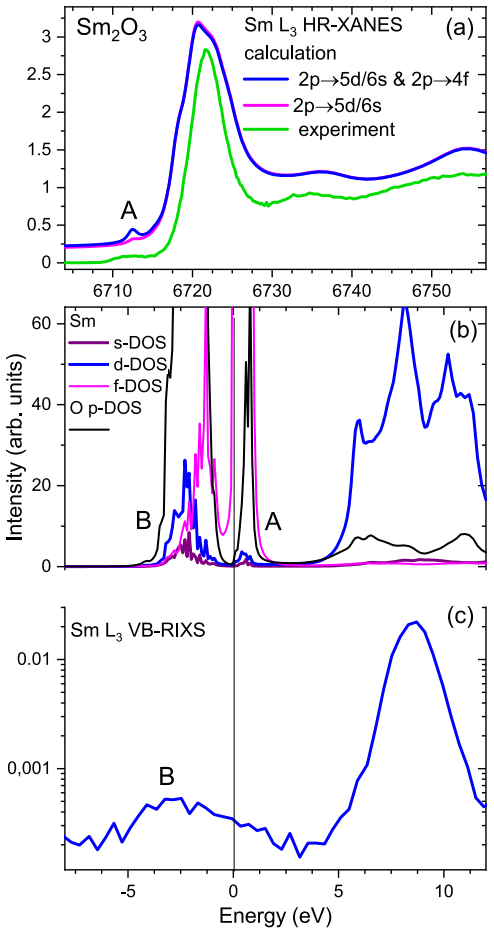

Figure 2. (a) Sm L_3-edge HR-XANES experimental and computed spectra of Sm_2O_3. (b) Selected computed angular momentum projected density of states (DOS) for Sm and O. All calculations are performed with the FDMNES code. (c) Sm L_3-edge VB-RIXS spectrum of Sm_2O_3. The vertical line divides the occupied states from the unoccupied states.

no intensity would be observable in this energy region as there is no 6s or 5d electron density in the valence band. However, there is a clear peak in the VB-RIXS spectrum of Sm_2O_3, which provides evidence that the Sm−O bonds have some covalent character with participation of 5d and 6s electrons, resulting in the 5d and 6s electron densities observed in peak B.

The DFT-based finite difference method for near-edge structure (FDMNES) calculations of the angular momentum-projected DOS reveals O 2p and Sm 5d, 4f and 6s states within a similar energy region, indicating mixing of these orbitals. The overlap of orbitals evaluated with the FDMNES code (Coop tool) confirms this notion (cf. Supporting Information (SI) Figure S1). This tool integrates the number of electrons between two bonding atoms in specific orbitals and thus gives a quantitative measure of the bond covalency. Considering the theoretical and experimental results, we conclude that there is electron redistribution between the 4f, 6s, and 5d orbitals of Sm, resulting in covalent Sm−O bonding.

Bond Covalency in $[Sm(\eta^9\text{-}C_9H_9)_2]$. Given the novel results of investigations into Sm_2O_3, we then studied the mixing of Sm 5d/6s and O 2p orbitals in the Sm(II) molecular compound $[Sm(\eta^9\text{-}C_9H_9)_2]$. Sm L_3-edge HR-XANES spectra of $[Sm(\eta^9\text{-}C_9H_9)_2]$ from both FDMNES calculations and experimental measurements are depicted in Figure 3a and the

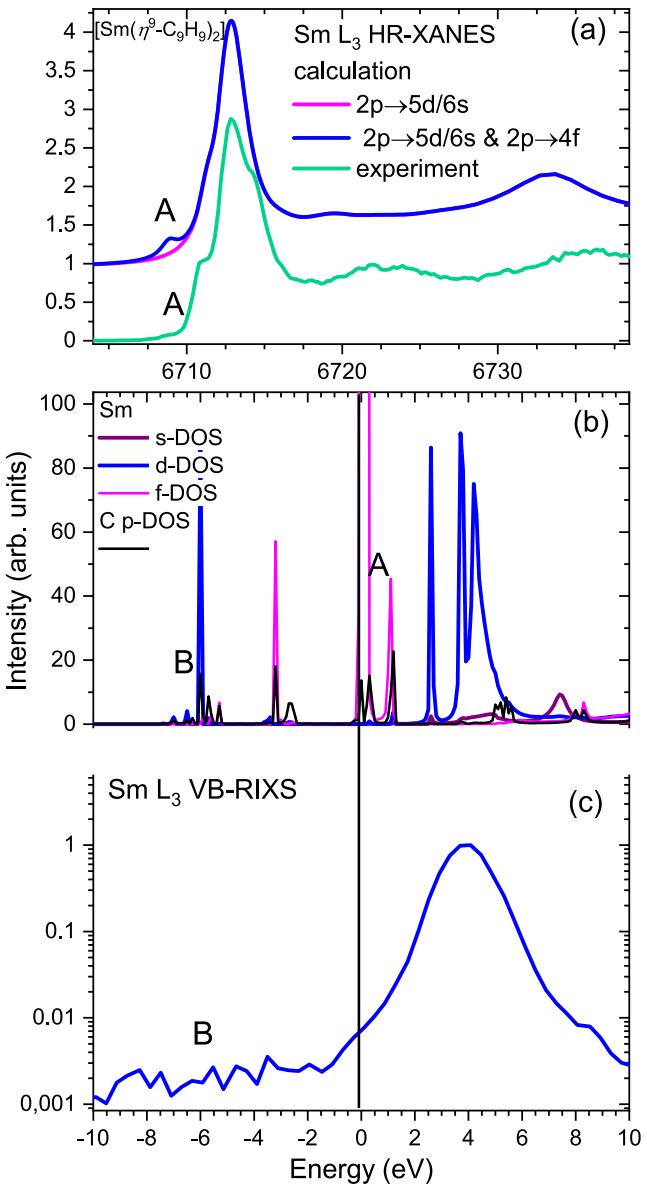

Figure 3. (a) Sm L_3-edge HR-XANES experimental and computed spectra of $[Sm(\eta^9\text{-}C_9H_9)_2]$. (b) Selected computed angular momentum projected density of states (DOS) for Sm and O. All calculations are performed with the FDMNES code. (c) Sm L_3-edge VB-RIXS spectra. The vertical line divides the occupied from the unoccupied states.

theoretical DOS in Figure 3b. The calculation once again reproduces all spectral features (Figure 3a). The shoulder on the high energy side of the main peak at 6714.34 eV is visible in the d-DOS but not resolved in the theoretical spectrum after broadening of the spectral features. This is the first example of an experimental Sm(II) L_3-edge HR-XANES spectrum recorded with sufficiently high energy resolution that the pre-edge peak A is resolved. This pre-edge peak is not present when we include only electric-dipole transitions (2p → 5d/6s) in the calculation of the Sm L_3-edge HR-XANES spectrum, which suggests that the pre-edge feature is predominantly caused by transitions to 4f orbitals (2p → 4f), i.e., electric-quadrupole transitions. This result shows that no substantial mixing of 5d/6s and 4f orbitals occurs due to the high symmetry structure of $[Sm(\eta^9\text{-}C_9H_9)_2]$ belonging to either the D_{9h} or D_{9d} point groups (cf. Tables S2 and S3). The calculated occupied DOS in Figure 3b also shows a small d contribution and only a minor mixing of metal with ligand orbitals. This result is confirmed by the Sm and C DOS calculated for the ground and excited state with the Amsterdam Density Functional Theory (ADF) code[28] presented in the SI Figure S2a. The Sm L_3-edge VB-RIXS spectrum depicted in Figure 3c has an intense elastic scattering peak and no noticeable intensity in energy region B, in contrast to Sm_2O_3, confirming that no significant 5d/6s contribution is present in the Sm−C bonds. The molecular orbital scheme of $[Sm(\eta^9\text{-}C_9H_9)_2]$ is shown in SI Figures S3 and S4.

The orbital population analyses performed with ADF are in accordance with the DOS and the VB-RIXS results. The occupied valence orbitals have predominantly ligand character with up to 6% Sm 4f and up to 7% Sm 5d participation (cf. Figure S10, Tables S4, and S5). We define bond covalency in terms of mixing coefficients between ligand orbitals and Sm 4f and 5d valence orbitals, which is in theory proportional to the overlap integrals and inversely proportional to the energy difference between Sm 4f/5d and C $2p_z$ valence orbitals.[16] All findings reveal the ionic character of the Sm−ligand chemical bond, as previously reported by Xemard et al.[21]

Photon-Induced Bond Covalency in $[Sm(\eta^9\text{-}C_9H_9)_2]$. *Sm L_3-edge HR-XANES of $[Sm(\eta^9\text{-}C_9H_9)_2]$.* Upon X-ray irradiation, the intensity of the Sm(II) main absorption peak in the HR-XANES spectrum reduces, and at the same time, a strong absorption feature starts to appear at about 6722 eV, which has a similar energy position to the main absorption peak of Sm_2O_3. This observation shows that the Sm 2p core−hole created in the excitation process is poorly screened, compared to the ground state, since the electron density from Sm 4f orbitals is transferred to either 5d/6s-based orbitals or the ligand (cf. Figures 4a and 7a, peak D). Calculated excitation energies of $[Sm(\eta^9\text{-}C_9H_9)_2]$ in Figure 5 show that the $4f^5 5d^1$ multiplets of Sm(II) are overlaying the $4f^6$ states, indicating that electron transfer from 4f to 5d states is energetically possible in $[Sm(\eta^9\text{-}C_9H_9)_2]$. More energy is required for ligand-to-metal charge transfer (LMCT), and thus, LMCT is less probable (cf. Figure 5). It has been reported previously that 4f → 5d transitions are present in Sm(II) crown ether compounds using photoluminescence experiments. Here, the Sm $4f^6$ and $4f^5 5d^1$ multiplets were obtained by applying the ligand-field density-functional theory (LFDFT) method in ADF.[28] In addition, we used the time-dependent DFT (TDDFT) formalism in ADF for calculating excitation energies that belong to LMCT as well as metal-to-ligand charge transfer (MLCT) and ligand $\pi-\pi^*$ following a similar methodology that is already detailed elsewhere[29] (cf. SI Sections 3 and 6). The ADF calculations report −0.06 Å shorter Sm−C_9H_9 bond length going from Sm $4f^6$ to Sm $4f^5 5d^1$ electronic configuration (cf. Figure 6a and Tables S2 and S3).

Note that when exposed to an ambient atmosphere, $[Sm(\eta^9\text{-}C_9H_9)_2]$ oxidizes to Sm_2O_3 (cf. Figure S6). Photoinduced activation of Sm $4f^6 \rightarrow 4f^5 5d^1$ followed by reaction with oxygen is unlikely to occur since the sample was sealed in a borosilicate glass capillary. We also repeated the experiments at different beamlines and synchrotrons measuring multiple samples, and these results were repeatable. The reaction of Sm with a small amount of moisture or oxygen present in the sample can be excluded as demonstrated by the Sm L_3-edge HR-XANES spectra in Figure 4. The trend in the changes of the postedge features upon X-ray irradiation of the compound

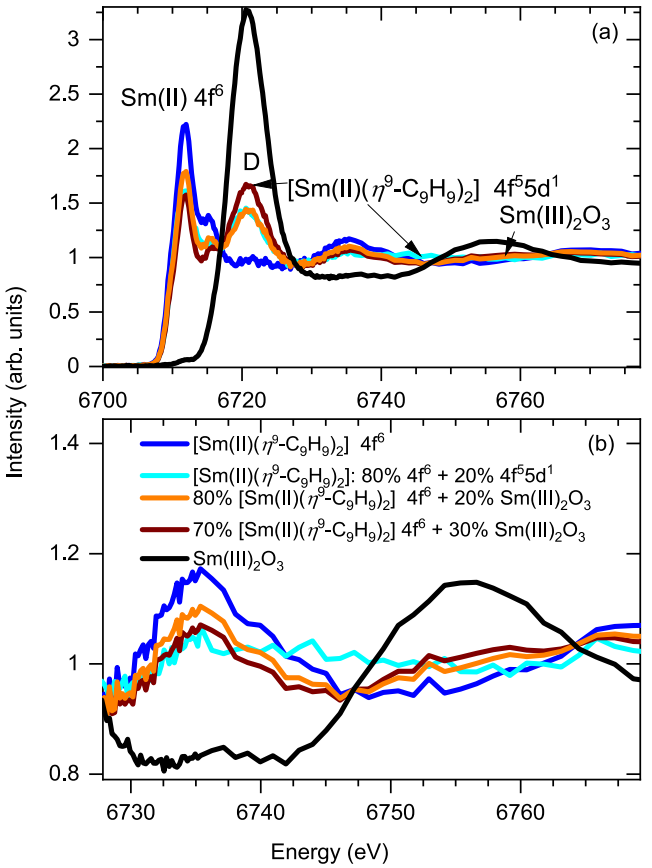

Figure 4. Sm L_3-edge HR-XANES experimental spectra of [Sm(η^9-$C_9H_9)_2$] for Sm $4f^6$, and a mixture of Sm $4f^6$ and $4f^55d^1$ configurations as well as a linear combination of 80/70% Sm_2O_3 and 20/30% [Sm(η^9-$C_9H_9)_2$] $4f^6$ spectra. Panel (a) shows the complete spectra and panel (b) depicts only the postedge region of the spectra.

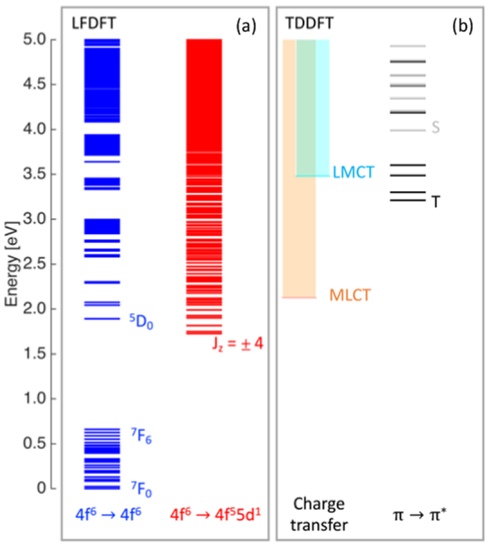

Figure 5. Calculated ground and low-lying excited states of [Sm(η^9-$C_9H_9)_2$] obtained from the LFDFT and TDDFT methods. Note that energy levels are shown in a bar diagram: multiplet structure and ligand-field interaction of Sm $4f^6$ (in blue) and Sm $4f^55d^1$ (in red) configurations, as well as charge transfer energies corresponding to the ligand-to-metal (LMCT in cyan), metal-to-ligand (MLCT in orange), and ligand π–π^* singlet (S) and triplet (T) states (in gray).

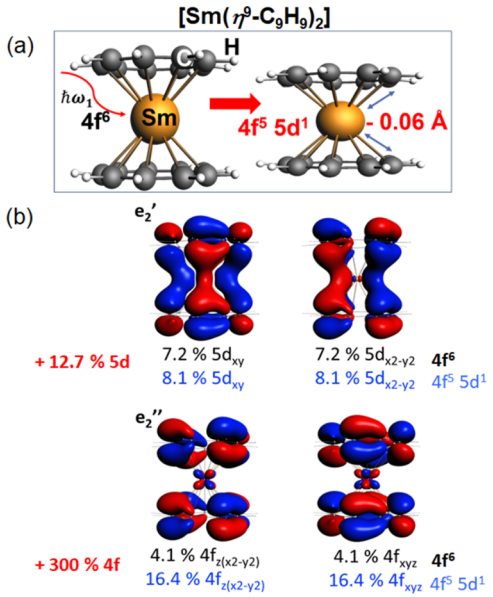

Figure 6. (a) [Sm(η^9-$C_9H_9)_2$] structural scheme before and after X-ray irradiation. (b) Selected double occupied Kohn–Sham molecular orbitals of [Sm(η^9-$C_9H_9)_2$], showing the change of Sm 5d and 4f contributions in the molecular orbitals when going from Sm $4f^6$ to Sm $4f^55d^1$ electron configuration.

is not characteristic for Sm_2O_3 (cf. Figure 4b). In order to demonstrate this more clearly, we simulated Sm L_3-edge HR-XANES spectra, which are linear combinations of [Sm(η^9-$C_9H_9)_2$] $4f^6$ and the Sm_2O_3 spectra (cf. Figure 4). It is clearly visible that the change in the simulated spectra is at different energy position compared to the spectral change going from [Sm(η^9-$C_9H_9)_2$] $4f^6$ to [Sm(η^9-$C_9H_9)_2$] $4f^55d^1$ configuration. The photoinduced change of electron configuration from [Sm(η^9-$C_9H_9)_2$] $4f^6$ to [Sm(η^9-$C_9H_9)_2$] $4f^55d^1$ is partial and is independent of the irradiation time. We found that the Sm $4f^55d^1$ configuration contributes up to 20% considering the intensity of peak D characteristic for the Sm $4f^55d^1$ configuration. The process is not reversible by turning off the X-ray beam and keeping the sample for about three months in the dark. This demonstrates that the electron density transferred from 4f to 5d orbitals activated Sm and led to an irreversible follow-up reaction.

Sm L_3-edge EXAFS. Recently, we showed for Ln(III) bound to n-Pr-BTP [2,6-bis(5,6-dipropyl-1,2,4-triazin-3-yl)-pyridine] that the Ln L_3-edge HR-XANES postedge spectral features are very sensitive to changes of the coordination environment, including bond angles and bond lengths, and thus to structural changes due to potential bond dissociation.[23] In the current study, there is reduction of amplitudes of the oscillations in the postedge region of the Sm L_3-edge HR-XANES spectrum, which is an indication for reduced coordination numbers and structural disorder but dissociation of the molecule is unlikely (cf. Figures 4, 7a, S6, and S7). We recorded Sm L_3-edge EXAFS spectra for [Sm(η^9-$C_9H_9)_2$] $4f^6$ and a mixture of [Sm(η^9-$C_9H_9)_2$] $4f^6$ and [Sm(η^9-$C_9H_9)_2$] $4f^55d^1$ configurations to study in detail the changes in the local coordination environment of Sm. The first coordination sphere of Sm was modeled considering one or two Sm–C scattering paths. The model including two Sm–C scattering paths is more realistic since the crystal structure contains 18 C first neighboring atoms of Sm at distances within 2.87–2.96 Å (2.90 Å average

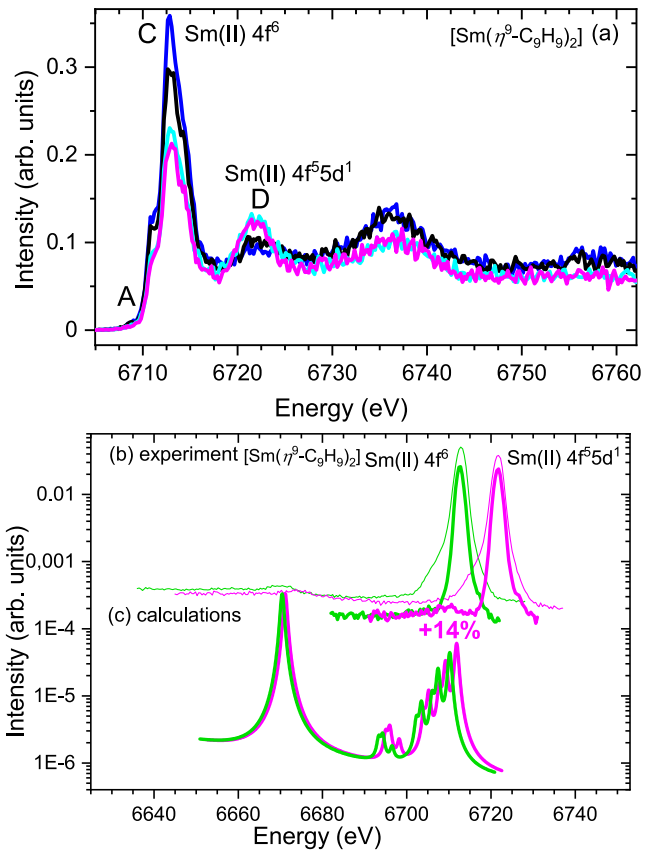

Figure 7. (a) Sm L_3-edge HR-XANES spectra of $[Sm(\eta^9\text{-}C_9H_9)_2]$, showing systematic changes from the Sm(II) $4f^6$ to Sm(II) $4f^5 5d^1$ electron configuration upon X-ray irradiation. Each spectrum is measured for 20 s on the same sample spot. The Sm L_3-edge VB-RIXS (b) experimental and (c) computed spectra with the ADF code of $[Sm(\eta^9\text{-}C_9H_9)_2]$ representative of the two different valence electron configurations are displayed. The experimental spectra are measured for two experimental energy resolutions and energy ranges. The intensities of both experimental and computed spectra increase upon X-ray irradiation (spectra in magenta). The calculations reveal 14% higher intensity, corroborating that the electron transfer from 4f to 5d orbitals takes place.

bond length). The best fit to the experimental Sm L_3-edge FT-EXAFS spectrum of the mixed configuration (including both $[Sm(\eta^9\text{-}C_9H_9)_2]$ $4f^6$ and $[Sm(\eta^9\text{-}C_9H_9)_2]$ $4f^5 5d^1$) reveals shorter Sm−C bond lengths (Sm−C1−0.9 ± 0.05 Å, Sm−C2−0.4 ± 0.02 Å), reduced coordination numbers for the C1 atoms (Sm−C1−5 ± 1, Sm−C2−1 ± 1), and increased Debye−Waller factor compared to the EXAFS results for $[Sm(\eta^9\text{-}C_9H_9)_2]$ $4f^6$, supporting the DFT results and suggesting structural disorder for the mixed configuration containing $[Sm(\eta^9\text{-}C_9H_9)_2]$ $4f^6$ and $[Sm(\eta^9\text{-}C_9H_9)_2]$ $4f^5 5d^1$ (cf. Table S6, Figures S8 and S9).

Sm L_3-edge HR-XANES Simulations. The FDMNES calculations of the Sm L_3-edge HR-XANES spectra for variable Sm−C_9H_9 bond lengths and for only one Sm−C_9H_9 bond support the EXAFS results that the Sm−C_9H_9 bond length shortens and structural disorder leads to reduced C coordination numbers (cf. Figures S11). The postedge spectral features slightly shift to higher energy for shorter bond lengths (Figure S11a,b) and the amplitude of the peaks reduces when the coordination number decreases (Figure S11d). Both changes are observed in the experimental Sm L_3-edge HR-XANES spectrum for the mixed configuration $[Sm(\eta^9\text{-}C_9H_9)_2]$ $4f^6$ and $[Sm(\eta^9\text{-}C_9H_9)_2]$ $4f^5 5d^1$ (cf. Figures 4, 7a, S6, and S7). Bending of the molecule from 180° to 150° does not lead to substantial changes of the spectrum (cf. Figure S11c).

Sm L_3-edge VB-RIXS of $[Sm(\eta^9\text{-}C_9H_9)_2]$. VB-RIXS can further elucidate the change in bonding in the $[Sm(\eta^9\text{-}C_9H_9)_2]$ molecule upon X-ray irradiation. The VB-RIXS spectra measured by selectively exciting only the Sm(II) $4f^6$ configuration are shown in Figures 3c and 7b (green spectrum). This is achieved by tuning the excitation energy to the most intense absorption feature, peak C, of the Sm(II) $4f^6$ L_3-edge HR-XANES (cf. Figure 7a). The VB-RIXS spectra in Figure 7b are recorded with two different experimental energy resolutions (3/1.8 eV) and illustrate that there are no significant 5d and 6s contributions in the occupied valence orbitals of $[Sm(\eta^9\text{-}C_9H_9)_2]$. However, the peak probing the Sm 5d and 6s electron density in the valence band increases in intensity when electrons are selectively excited from the Sm(II) $4f^6$ to the Sm(II) $4f^5 5d^1$ electron configuration. This was recorded by setting the excitation energy at the maximum of peak D characteristic for the Sm(II) $4f^5 5d^1$ electron configuration (cf. Figure 6a).

The increase of intensity in the occupied valence band for the VB-RIXS maps of Sm(II) $4f^5 5d^1$ shown in Figure 8b

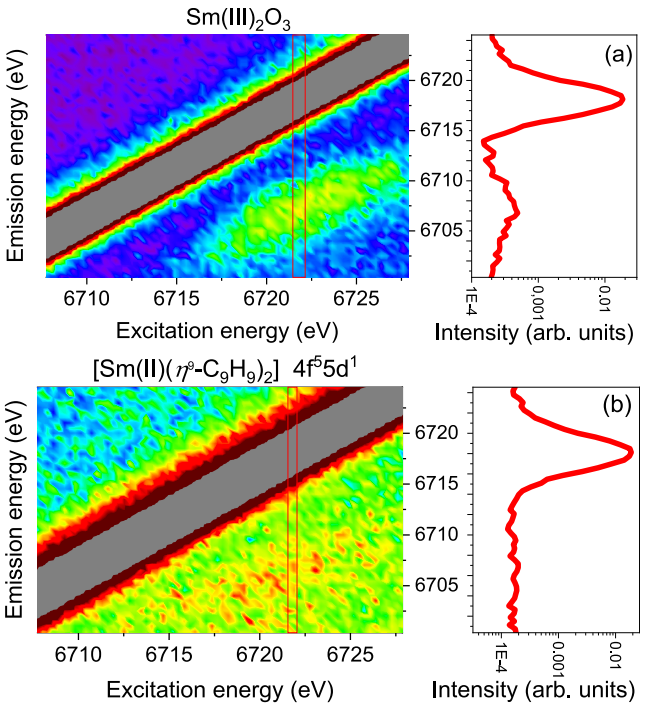

Figure 8. Sm L_3-edge VB-RIXS maps and cross sections at constant excitation energy at the energy position of peak D shown in Figure 7a of Sm_2O_3 (a) and $[Sm(\eta^9\text{-}C_9H_9)_2]$ for Sm $4f^5 5d^1$ (b).

demonstrates that upon X-ray radiation, the electron density transfers from 4f to 5d orbitals, which then participate in the binding and are involved in covalent bonding interaction with the ligand. The computed VB-RIXS spectra show about 14% of total increase of 5d/6s intensity in the occupied valence band corroborating the experimental result (cf. Figure 7c). The specific occupied valence band orbitals and the change in relative Sm f/d contributions are listed in Figure 6b. It is also remarkable that in the Sm(II) $4f^5 d^1$ configuration, the 4f

contributions in the e_2'' occupied orbitals increase by 300% (cf. Figures 6b and S10). This Sm 4f contribution is also visible in the occupied valence DOS calculated by ADF for the Sm(II) $4f^5d^1$ configuration shown in Figure S2.

SUMMARY AND CONCLUSIONS

We probed the electron density in the Sm 4f/5d/6s unoccupied and occupied valence states of the $[Sm(\eta^9\text{-}C_9H_9)_2]$ molecule and Sm_2O_3 solid compound by performing Sm L_3-edge HR-XANES and VB-RIXS spectroscopy and computations. It was demonstrated that Sm(III) forms covalent bonds with O in Sm_2O_3 induced by mixing of Sm 6s, 5d, minor 4f and O 2p valence orbitals. Using our spectroscopic and theoretical approaches, we confirmed that $[Sm(\eta^9\text{-}C_9H_9)_2]$ exhibits ionic binding previously reported by quantum chemical computations. However, we showed that upon X-ray irradiation, Sm(II) pumps 4f electrons to 5d orbitals (Sm(II) $4f^6 \rightarrow 4f^5 5d^1$), triggering increased covalency of Sm−C bonds. In addition, Sm 4f electrons become substantially involved in covalent chemical bonding, as suggested by the ADF calculations. This theoretical prediction can be probed experimentally in further studies, applying Sm $M_{4,5}$-edges VB-RIXS spectroscopic technique sensitive to the Sm f electron density in the occupied valence band.

This drastic change in the Sm electronic structure in $[Sm(\eta^9\text{-}C_9H_9)_2]$ occurs without dissociation of the chemical bond. A small change of −0.06 Å in Sm−C bond lengths was calculated by ADF for Sm(II) $4f^5 5d^1$ compared to Sm(II) $4f^6$. We showed experimentally that this Sm $4f^6 \rightarrow 4f^5 5d^1$ charge transfer activates $[Sm(\eta^9\text{-}C_9H_9)_2]$, which is a robust Sm(II) compound, leading to a follow-up reaction. Sm L_3-edge EXAFS and HR-XANES analyses suggest that the resulting compound comprises about 20% of the probed sample and its geometric structure is very similar to $[Sm(\eta^9\text{-}C_9H_9)_2]$ but with increased structural disorder and shorter Sm−C bond lengths. This compound has detectable covalency of the Sm−C chemical bonds with 5d and 4f participation. Further studies will reveal if different ligand environments can fine-tune this charge transfer mechanism, leading to unusual Sm(II) bonding properties and reactivity.

AUTHOR INFORMATION

Corresponding Author

T. **Vitova** − *Institute for Nuclear Waste Disposal (INE), Karlsruhe Institute of Technology, D-76021 Karlsruhe, Germany;* orcid.org/0000-0002-3117-7701; Email: tonya.vitova@kit.edu

Authors

H. Ramanantoanina − *Institute for Nuclear Waste Disposal (INE), Karlsruhe Institute of Technology, D-76021 Karlsruhe, Germany*

B. Schacherl − *Institute for Nuclear Waste Disposal (INE), Karlsruhe Institute of Technology, D-76021 Karlsruhe, Germany;* orcid.org/0000-0003-4542-0108

L. Münzfeld − *Institute for Inorganic Chemistry, Karlsruhe Institute of Technology, D-76021 Karlsruhe, Germany*

A. Hauser − *Institute for Inorganic Chemistry, Karlsruhe Institute of Technology, D-76021 Karlsruhe, Germany*

R. S. K. Ekanayake − *Institute for Nuclear Waste Disposal (INE), Karlsruhe Institute of Technology, D-76021 Karlsruhe, Germany;* orcid.org/0000-0002-5255-1969

C. Y. Reitz − *Institute for Nuclear Waste Disposal (INE), Karlsruhe Institute of Technology, D-76021 Karlsruhe, Germany*

T. Prüßmann − *Institute for Nuclear Waste Disposal (INE), Karlsruhe Institute of Technology, D-76021 Karlsruhe, Germany;* orcid.org/0000-0002-7903-9199

T. S. Neill − *Institute for Nuclear Waste Disposal (INE), Karlsruhe Institute of Technology, D-76021 Karlsruhe, Germany;* Present Address: Department of Earth and Environmental Sciences, University of Manchester, Manchester, U.K; orcid.org/0000-0002-4316-1328

J. Göttlicher − *Institute for Photon Science and Synchrotron Radiation, Karlsruhe Institute of Technology, D-76021 Karlsruhe, Germany*

R. Steininger − *Institute for Photon Science and Synchrotron Radiation, Karlsruhe Institute of Technology, D-76021 Karlsruhe, Germany*

V. A. Saveleva − *ESRF, The European Synchrotron, 38043 Grenoble Cedex 9, France;* orcid.org/0000-0002-8221-4576

M. W. Haverkort − *Institute for Theoretical Physics, University of Heidelberg, D-69120 Heidelberg, Germany;* orcid.org/0000-0002-7216-3146

P. W. Roesky − *Institute for Inorganic Chemistry and Institute of Nanotechnology (INT), Karlsruhe Institute of Technology, D-76021 Karlsruhe, Germany;* orcid.org/0000-0002-0915-3893

Author Contributions

This manuscript was written through contributions of all authors. All authors have given approval to the final version of the manuscript.

Funding

This work received funding from Deutsche Forschungsgemeinschaft (DFG, German Research Foundation) through the Collaborative Research Centre "4f for Future" project A1 (CRC 1573, project number 471424360).

Notes

The authors declare no competing financial interest.

ACKNOWLEDGMENTS

The authors gratefully acknowledge financial support from the Deutsche Forschungsgemeinschaft (DFG, German Research Foundation) through the Collaborative Research Centre "4f for Future" project A1 (CRC 1573, project number 471424360). We acknowledge the high-performance comput-

ing (HPC) support, time, and infrastructure provided by SURFsara HPC at Snellius via the HPC-Europa3 program. We thank the Institute for Beam Physics and Technology (IBPT) for the operation of the storage ring, the Karlsruhe Research Accelerator (KARA). We thank the KIT Light Source for provision of beamtime. We acknowledge the European Synchrotron Radiation Facility for provision of beamtime at the ID26 beamline.

ABBREVIATIONS

HR-XANES, high-energy resolution X-ray absorption near-edge structure; VB-RIXS, valence band resonant inelastic X-ray scattering; DFT, density functional theory; LFDFT, ligand-field density functional theory; FDMNES, finite difference method near-edge structure; ADF, Amsterdam Density Functional; DOS, density of states

REFERENCES

(1) Zhang, W.; Muhtadi, A.; Iwahara, N.; Ungur, L.; Chibotaru, L. F. Magnetic Anisotropy in Divalent Lanthanide Compounds. *Angew. Chem., Int. Ed.* **2020**, *59* (31), 12720−12724.

(2) Cheng, X.; Zhou, J.; Yue, J.; Wei, Y.; Gao, C.; Xie, X.; Huang, L. Recent Development in Sensitizers for Lanthanide-Doped Upconversion Luminescence. *Chem. Rev.* **2022**, *122* (21), 15998−16050.

(3) Woodruff, D. N.; Winpenny, R. E. P.; Layfield, R. A. Lanthanide Single-Molecule Magnets. *Chem. Rev.* **2013**, *113* (7), 5110−5148.

(4) Qiao, Y.; Schelter, E. J. Lanthanide Photocatalysis. *Acc. Chem. Res.* **2018**, *51* (11), 2926−2936.

(5) Reddy, M. L. P.; Bejoymohandas, K. S.; Divya, V. Luminescent lanthanide coordination compounds as potential mitochondria-targeting probes: Molecular engineering to bioimaging. *Dyes Pigm.* **2022**, *205*, No. 110528.

(6) Daumann, L. J.; Pol, A.; Op den Camp, H. J. M.; Martinez-Gomez, N. C. A Perspective on the Role of Lanthanides in Biology: Discovery, Open Questions and Possible Applications. In *Advances in Microbial Physiology*; Poole, R. K.; Kelly, D. J., Eds.; Academic Press, 2022; Vol. *81*, pp 1−24.

(7) Löble, M. W.; Keith, J. M.; Altman, A. B.; Stieber, S. C.; Batista, E. R.; Boland, K. S.; Conradson, S. D.; Clark, D. L.; Lezama Pacheco, J.; Kozimor, S. A.; et al. Covalency in lanthanides. An X-ray absorption spectroscopy and density functional theory study of $LnCl_6^{x-}$ (x = 3, 2). *J. Am. Chem. Soc.* **2015**, *137* (7), 2506−2523.

(8) Minasian, S. G.; Batista, E. R.; Booth, C. H.; Clark, D. L.; Keith, J. M.; Kozimor, S. A.; Lukens, W. W.; Martin, R. L.; Shuh, D. K.; Stieber, S. C. E.; et al. Quantitative Evidence for Lanthanide-Oxygen Orbital Mixing in CeO_2, PrO_2, and TbO_2. *J. Am. Chem. Soc.* **2017**, *139* (49), 18052−18064.

(9) Fieser, M. E.; Ferrier, M. G.; Su, J.; Batista, E.; Cary, S. K.; Engle, J. W.; Evans, W. J.; Pacheco, J. S. L.; Kozimor, S. A.; Olson, A. C.; et al. Evaluating the electronic structure of formal Ln^{II} ions in $Ln^{II}(C_5H_4SiMe_3)_3^{1-}$ using XANES spectroscopy and DFT calculations. *Chem. Sci.* **2017**, *8* (9), 6076−6091.

(10) Smiles, D. E.; Batista, E. R.; Booth, C. H.; Clark, D. L.; Keith, J. M.; Kozimor, S. A.; Martin, R. L.; Minasian, S. G.; Shuh, D. K.; Stieber, S. C. E.; Tyliszczak, T. The duality of electron localization and covalency in lanthanide and actinide metallocenes. *Chem. Sci.* **2020**, *11* (10), 2796−2809.

(11) Tricoire, M.; Mahieu, N.; Simler, T.; Nocton, G. Intermediate Valence States in Lanthanide Compounds. *Chem.—Eur. J.* **2021**, *27* (23), 6860−6879.

(12) Poe, T. N.; Beltrán-Leiva, M. J.; Celis-Barros, C.; Nelson, W. L.; Sperling, J. M.; Baumbach, R. E.; Ramanantoanina, H.; Speldrich, M.; Albrecht-Schönzart, T. E. Understanding the Stabilization and Tunability of Divalent Europium 2.2.2B Cryptates. *Inorg. Chem.* **2021**, *60* (11), 7815−7826.

(13) Gompa, T. P.; Greer, S. M.; Rice, N. T.; Jiang, N. X.; Telser, J.; Ozarowski, A.; Stein, B. W.; La Pierre, H. S. High-Frequency and -Field Electron Paramagnetic Resonance Spectroscopic Analysis of Metal-Ligand Covalency in a 4f Valence Series (Eu, Gd, and Tb). *Inorg. Chem.* **2021**, *60* (12), 9064−9073.

(14) Vitova, T.; Roesky, P. W.; Dehnen, S. Open questions on bonding involving lanthanide atoms. *Commun. Chem.* **2022**, *5* (1), 12 DOI: 10.1038/s42004-022-00630-6.

(15) Wilson, H. H.; Yu, X. J.; Cheisson, T.; Smith, P. W.; Pandey, P.; Carroll, P. J.; Minasian, S. G.; Autschbach, J.; Schelter, E. J. Synthesis and Characterization of a Bridging Cerium(IV) Nitride Complex. *J. Am. Chem. Soc.* **2023**, *145* (2), 781−786.

(16) Neidig, M. L.; Clark, D. L.; Martin, R. L. Covalency in f-element complexes. *Coord. Chem. Rev.* **2013**, *257* (2), 394−406.

(17) Yoshimura, A.; Tomisaka, Y.; Li, Z.; Nomoto, A.; Ogawa, A. Photoinduced Reductive Coupling of Organochlorosilanes with SmI_2/Sm. *Heteroat. Chem.* **2014**, *25* (6), 684−689.

(18) Ogawa, A.; Ohya, S.; Sumino, Y.; Sonoda, N.; Hirao, T. Novel enhancement of the reducing ability of ytterbium diiodide by irradiation with near-UV light. *Tetrahedron Lett.* **1997**, *38* (52), 9017−9018.

(19) Ogawa, A.; Sumino, Y.; Nanke, T.; Ohya, S.; Sonoda, N.; Hirao, T. Photoinduced Reduction and Carbonylation of Organic Chlorides with Samarium Diiodide. *J. Am. Chem. Soc.* **1997**, *119* (11), 2745−2746.

(20) Schäfer, S.; Kaufmann, S.; Rösch, E. S.; Roesky, P. W. Divalent metallocenes of the lanthanides − a guideline to properties and reactivity. *Chem. Soc. Rev.* **2023**, *52* (12), 4006−4045.

(21) Xémard, M.; Zimmer, S.; Cordier, M.; Goudy, V.; Ricard, L.; Clavaguéra, C.; Nocton, G. Lanthanidocenes: Synthesis, Structure, and Bonding of Linear Sandwich Complexes of Lanthanides. *J. Am. Chem. Soc.* **2018**, *140* (43), 14433−14439.

(22) Vitova, T.; Denecke, M. A.; Göttlicher, J.; Jorissen, K.; Kas, J. J.; Kvashnina, K.; Prüßmann, T.; Rehr, J. J.; Rothe, J. Actinide and lanthanide speciation with high-energy resolution X-ray techniques. *JPCS* **2013**, *430*, No. 012117.

(23) Pruessmann, T.; Nagel, P.; Simonelli, L.; Batchelor, D.; Gordon, R.; Schimmelpfennig, B.; Trumm, M.; Vitova, T. Opportunities and challenges of applying advanced X-ray spectroscopy to actinide and lanthanide N-donor ligand systems. *J. Synchrotron Rad.* **2022**, *29*, 53−66.

(24) Hämäläinen, K.; Siddons, D. P.; Hastings, J. B.; Berman, L. E. Elimination of the inner-shell lifetime broadening in x-ray-absorption spectroscopy. *Phys. Rev. Lett.* **1991**, *67*, 2850.

(25) Kvashnina, K. O.; Butorin, S. M.; Glatzel, P. Direct study of the f-electron configuration in lanthanide systems. *J. Anal. At. Spectrom.* **2011**, *26*, 1265.

(26) Goodwin, C. A. P.; Reant, B. L. L.; Kragskow, J. G. C.; DiMucci, I. M.; Lancaster, K. M.; Mills, D. P.; Sproules, S. Heteroleptic samarium halide complexes probed by fluorescence-detected L_3 -edge X-ray absorption spectroscopy. *Dalton Trans.* **2018**, *47*, 10613−10625.

(27) Vitova, T.; Faizova, R.; Amaro-Estrada, J. I.; Maron, L.; Pruessmann, T.; Neill, T.; Beck, A.; Schacherl, B.; Tirani, F. F.; Mazzanti, M. The mechanism of Fe induced bond stability of uranyl(v). *Chem. Sci.* **2022**, *13* (37), 11038−11047.

(28) Baerends, E. J. AMS2022. SCM Amsterdam. https://www.scm.com.

(29) Ramanantoanina, H.; Merzoud, L.; Muya, J. T.; Chermette, H.; Daul, C. Electronic Structure and Photoluminescence Properties of $Eu(\eta^9\text{-}C_9H_9)_2$. *J. Phys. Chem. A* **2020**, *124* (1), 152−164.